Evaluation of the Mechanical Properties and the Corrosion Resistance of the Cobalt-Base Alloy Stellite 6 on 1045 Steel by Laser Cladding

Thang Le Toan
Faculty of Mechanical Engineering, University of Transport and Communications, Hanoi, Vietnam | National Research Institute of Mechanical Engineering, Hanoi, Vietnam
thanglt@utc.edu.vn

Nguyen Van Cuong
Faculty of Mechanical Engineering, University of Transport and Communications, Hanoi, Vietnam
nguyencuong@utc.edu.vn (corresponding author)

Received: 20 February 2025 | Revised: 19 March 2025 | Accepted: 5 April 2025

 DOI: https://doi.org/10.48084/etasr.10654

ABSTRACT

This study investigates the optimization of laser cladding parameters for Stellite 6 coatings on 1045 steel through experimental trials, ensuring the selected parameters, such as laser power, scanning speed, and powder feed rate, are optimized under realistic processing conditions. The results demonstrate significant improvements in coating performance. The optimized process produced a refined dendritic microstructure with a uniform distribution of Co-γ and Cr_7C_3 phases, effectively minimizing defects and improving mechanical stability. The coating exhibited a 2.8-fold increase in microhardness compared to the uncoated substrate, translating to significantly improved wear resistance. Additionally, electrochemical corrosion tests in a 3.5 wt.% NaCl solution showed a 200-fold reduction in corrosion rate and a protection efficiency of 99.75%, surpassing previously reported coatings that suffered from excessive dilution and phase inhomogeneity. These findings underscore the potential of experimentally optimized laser cladding to significantly enhance the durability and functional performance of Stellite 6 coatings.

Keywords-laser cladding; Stellite 6; microstructure; microhardness; electrochemical corrosion

I. INTRODUCTION

With the continued advancement of industrialization, the demand for sustainable development has become a top priority. Applying coatings with superior mechanical properties to the surfaces of worn components or common substrate metals not only enables the reuse of discarded parts but also enhances their wear and corrosion resistance. This reflects the pivotal role of surface coatings in promoting sustainable manufacturing [1].

Currently, widely adopted surface coating technologies include electroplating, thermal spraying, overlay welding, and laser cladding [2–5]. Electroplating is favored for its high efficiency and low cost; however, its widespread use is increasingly restricted due to significant environmental concerns. Thermal spraying is also broadly used, yet its limitations include high porosity, coating defects, and the reliance on a mechanically bonded interface, which is often unstable. Overlay welding creates a metallurgical bond with the substrate but suffers from low precision and a high dilution ratio, ultimately affecting coating quality. With the emergence of automation, additive manufacturing technologies have gained popularity [6]. Among these, laser cladding stands out as a highly automated process that offers excellent coating quality, low dilution, and minimal distortion. In laser cladding, a high-energy laser beam is used to melt both the cladding material and the substrate, resulting in a solidified layer that is metallurgically bonded to the base material. This method provides several advantages, including high energy density, minimal thermal deformation, and strong interfacial bonding [7]. Cladding material can be supplied via two primary methods: pre-placed powder and coaxial powder feeding, with the latter being preferred due to its superior automation and efficiency [8]. In recent years, several studies have investigated laser cladding of alloy coatings on steel substrates. Authors in [9] studied the coaxial laser cladding of cobalt-based Stellite 6 alloy on gray cast iron substrate, analyzing the dependence of microstructure and mechanical properties on laser power. In [10], Ni35 powder was clad onto C45 steel, revealing the influence of scanning speed and powder feed rate on microstructure and hardness, as well as their effect on dilution and the heat-affected zone. Authors in [11] studied the microstructure and wear resistance of TiC coating on graphite nodular cast iron substrate using a pre-powder laser cladding method, resulting in substantial improvements in hardness and

wear resistance. In [12], laser cladding of Inconel 625 on AISI 304 stainless steel enhanced the coating's hardness by 1.5 times compared to the substrate. Similarly, authors in [13] reported significant improvement in corrosion resistance for Ni60CuMoW-coated 45 steel in a 3.5 wt.% NaCl solution. Lastly, authors in [14] demonstrated the excellent Vickers hardness and corrosion resistance achieved through graphene-based laser cladding on 45 carbon steel.

In the present work, Stellite 6—a cobalt-based superalloy—was deposited onto 1045 medium-carbon steel using laser cladding. Then, the resulting coating's mechanical properties and corrosion resistance were evaluated to assess the practical applicability of Stellite 6 for extending component life and advancing sustainable engineering solutions.

II. MATERIALS AND METHODS

The substrate used in this study was AISI 1045 steel (medium carbon steel) with dimensions of 150mm x 60mm x 20mm. The substrate was polished and cleaned with acetone before laser coating. The coating material was spherical Stellite 6, a cobalt-based alloy powder with a particle size range of 50–150 μm, dried for 30 minutes before coating. The chemical compositions of both the Stellite 6 powder and the 1045 steel substrate, as provided by the suppliers, are listed in Table I.

TABLE I. COATING POWDER AND SUBSTRATE CHEMICAL COMPOSITION (WT%)

Element	**Co**	**C**	**Si**	**Fe**	**Cr**	**Mn**	**Mo**	**W**
Stellite 6	Bal	1.1	1.0	1.5	28.5	1	1.2	4.2
Element	**Fe**	**C**	**Si**	**Mn**	**Cr**	**Ni**	**P**	**S**
1045 Steel	Bal	0.45	0.36	0.5	0.25	≤0.2	≤0.04	≤0.04

Laser cladding was carried out using a Yb-fiber laser system (Raycus RFL-C6000), equipped with a coaxial powder-feeding cladding head mounted on a three-axis CNC platform. The powder feeding system was controlled by a rotating disk and guided into the laser cladding head by argon gas. The laser coating process parameters were programmed and controlled via a computer. The parameters of the laser cladding process are shown in Table II.

TABLE II. THE PARAMETERS OF THE LASER CLADDING PROCESS

Parameters	**Value**
Laser power, kW	2000
Scanning speed, mm/min	800
Powder feeding rate, g/min	18
Powder feeding gas, l/min	7.2
Shielding gas, l/min	22
Laser spot size diameter, mm	3
Focus distance, mm	16
Overlapping ratio, %	50
Coating thickness, mm	2

The principle of the laser cladding process is illustrated in Figure 1(a). The cladding process, with parameters set according to Table II, is shown in Figure 1(b), and the sample after cladding is shown in Figure 1(c).

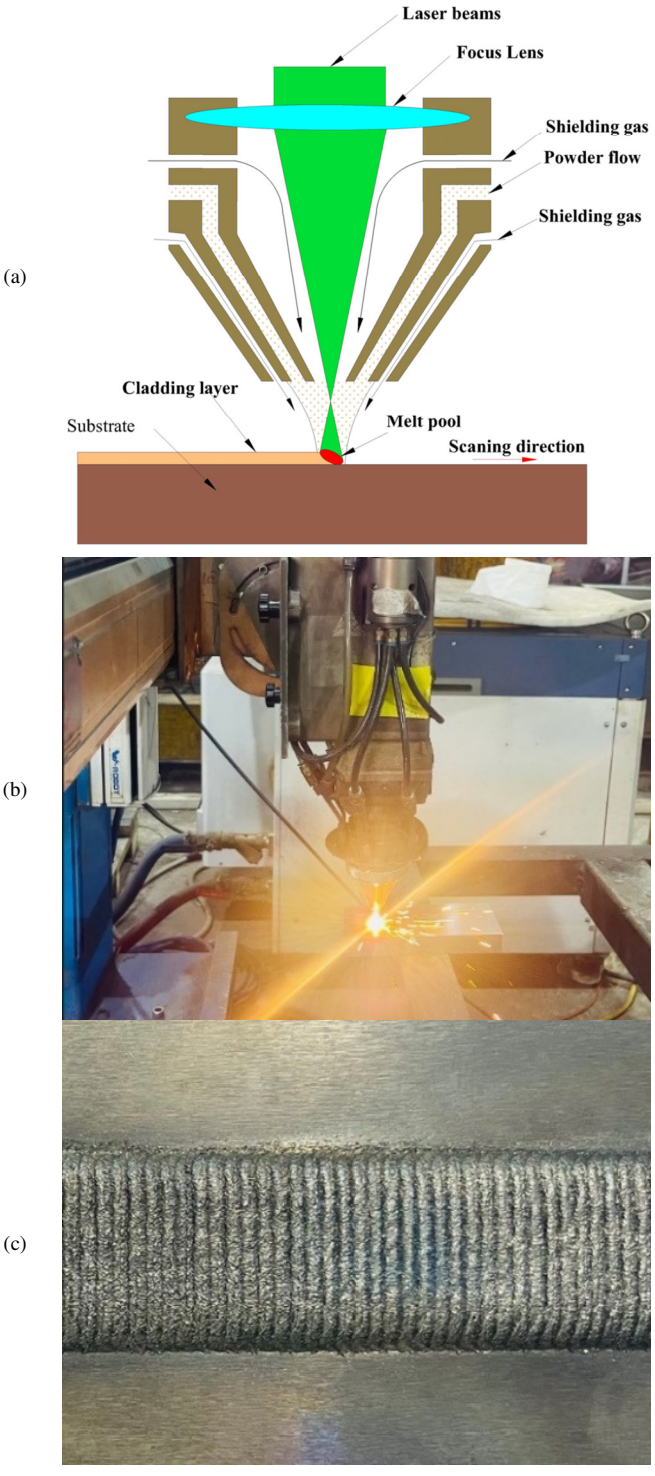

Fig. 1. Laser cladding process: (a) laser cladding principle; (b) experimental conduct; (c) a sample after laser cladding.

To determine the microstructure of the coating, the coated sample was cut using wire cutting and then polished with SiC sandpaper ranging from 1000 grit to 2000 grit. The surface was further polished with synthetic diamond powder and aluminum powder and finally cleaned with pure alcohol. The polished and

cleaned sample was dried in a vacuum oven for 30 minutes. To clearly distinguish the material zones and grain types, the sample surface was etched (Figure 2).

The Axiovert 40MAT optical microscope was used to examine the microstructure of the coating and interface region. The microhardness of the coating was measured using an IndentaMet 1106 hardness tester, following the ASTM E384-17 standard. A Vickers hardness test ($HV_{0.3}$) was used, with a 0.3 kgf load applied for 15 s. Hardness profiles were obtained by taking ten measurements—five across the coating and five across the substrate.

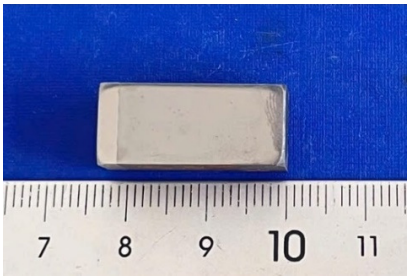

Fig. 2. Sample after preparation.

(a)

(b)

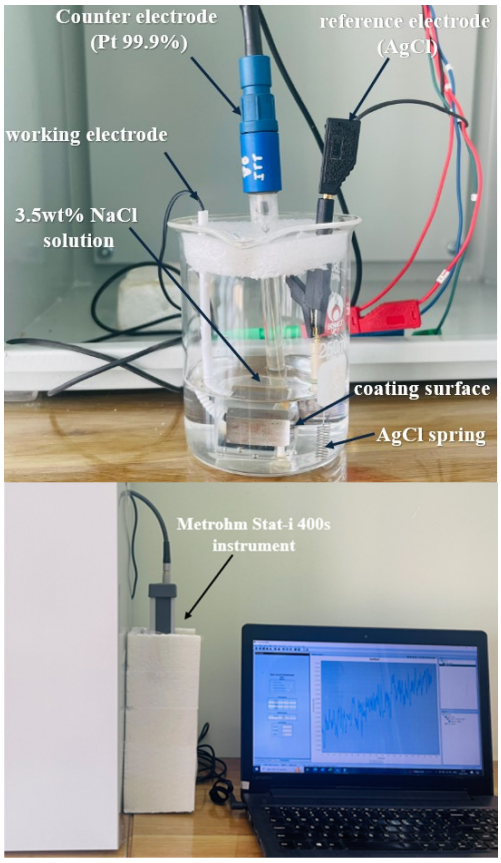

Fig. 3. (a) Electrochemical corrosion test setup, (b) electrochemical corrosion measurement process.

To measure the electrochemical corrosion resistance of the laser coating, the coating surface was prepared with dimensions of 10 mm x 10 mm. The surface was polished with sandpaper up to 2000 grit, followed by polishing with diamond and aluminum powder, then cleaned with alcohol and dried. An electrical wire was connected to the opposite side of the surface, while the remaining surfaces were covered with acrylic glue to prevent contact with the corrosive environment. The corrosion test was conducted in a 3.5 wt.% NaCl solution, simulating a seawater environment. Electrochemical corrosion resistance was measured using a Metrohm Stat-i 400s instrument with DropView 8400 software. The experimental setup and testing procedure are illustrated in Figures 3(a) and 3(b), respectively.

III. RESULTS AND DISCUSSION

A. *Microstructure Analysis*

Figure 4 shows the microstructure at the interface zone between the coating and the substrate, observed under a microscope at 500x magnification. The microstructure of the 1045 steel substrate consists of white ferrite (α-Fe) phases interspersed with brown pearlite phases, which is a typical morphology of medium-carbon steel when slowly cooled from the austenite (γ-Fe) region. At the coating–substrate interface, a planar microstructure with elemental diffusion can be observed, possibly containing a mixed phase of Fe-Co-Cr. No cracks or pores were detected at the interface between the coating and the substrate, indicating good metallurgical bonding.

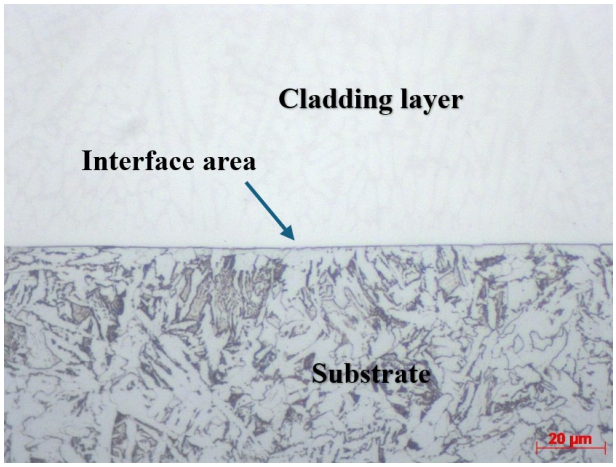

Fig. 4. The microstructure at the interface zone of the coating/substrate at 500x magnification.

The microstructure of the coating is shown in Figure 5. The image reveals a columnar dendritic structure, which is characteristic of rapidly solidified Stellite 6 alloy. The coating primarily consists of Co-γ phases (light background) interspersed with dark Cr_7C_3 carbide phases. Additionally, due to the presence of tungsten in the alloy, WC tungsten carbide phases may also be present. This Co-rich matrix provides high ductility and excellent corrosion resistance. The dendritic growth proceeds from the interface toward the coating surface, following the direction of the thermal gradient. The dendrites

are relatively fine and aligned in parallel bands, suggesting a rapid cooling rate and controlled solidification process. The uniformity and refinement of the dendrites indicate that the chosen laser cladding parameters effectively produced a dense, high-quality coating with an approximate thickness of 2 mm.

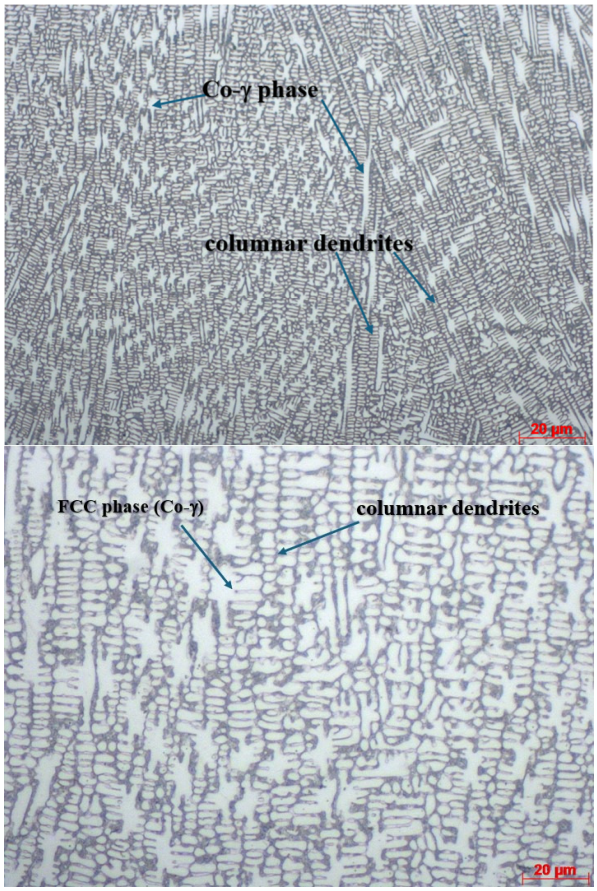

Fig. 5. The microstructure of the cladding layer: a) Microstructure of the coating at 200x magnification, b) microstructure of the coating at 500x magnification.

B. Microhardness

Figure 6 displays the Vickers microhardness profile measured across ten points from the coating surface through the interface to the substrate. The microhardness of the AISI 1045 steel substrate, based on five measurement points, averaged approximately 172.56 $HV_{0.3}$. The furthest measurement point from the interface zone has the lowest hardness of 168 $HV_{0.3}$, which gradually increases to 182.9 $HV_{0.3}$ at the point adjacent to the interface zone. This gradual increase in hardness toward the interface suggests the diffusion of alloying elements such as Co and Cr from the coating into the substrate, thereby enhancing the hardness of the adjacent substrate region.

In contrast, the five measurement points within the Stellite 6 cladding layer showed a significantly higher average microhardness of 481.64 $HV_{0.3}$. The hardness values across these points were relatively consistent, with the highest value observed at the third measurement point at 488.7 $HV_{0.3}$. This elevated hardness is primarily attributed to the presence of hard Cr_7C_3 carbide phases, contributing to the improved wear resistance of the coating. Notably, the measurement point closest to the interface recorded a hardness of 487 $HV_{0.3}$, slightly above the average value, indicating that Fe dilution from the substrate into the coating is minimal. This result confirms that the mechanical integrity and hardness of the coating near the interface are well preserved.

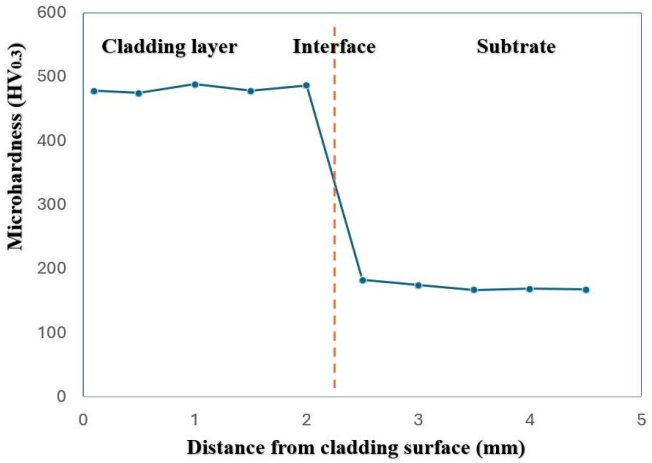

Fig. 6. Longitudinal Vickers microhardness diagram of Stellite 6 alloy laser cladding sample.

C. Electrochemical Corrosion Resistance

The electrochemical corrosion resistance of the Stellite 6 alloy laser coating was evaluated through electrochemical corrosion measurement experiments. Before conducting the corrosion measurement, the working electrode was immersed in 3.5 wt.% NaCl solution for 30 minutes to obtain a steady state of the measured values. Then, the open circuit potential (E_{ocp}) was measured, serving as a baseline for corrosion analysis. As shown in Figure 7, the E_{ocp} stabilized at approximately -0.185 V.

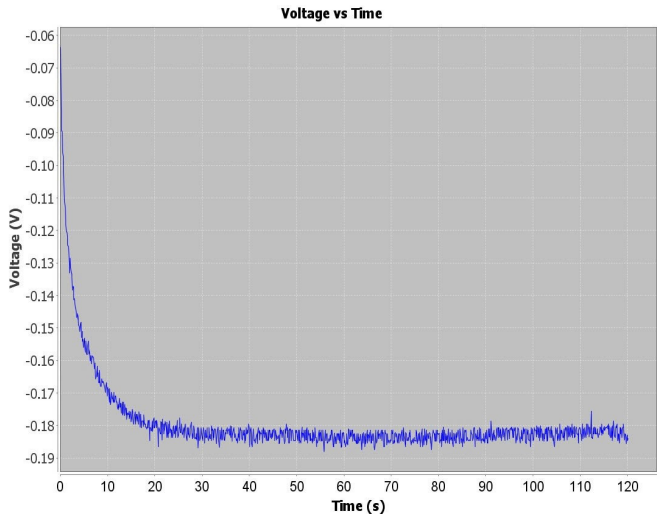

Fig. 7. Graph of the open circuit potential (E_{ocp}).

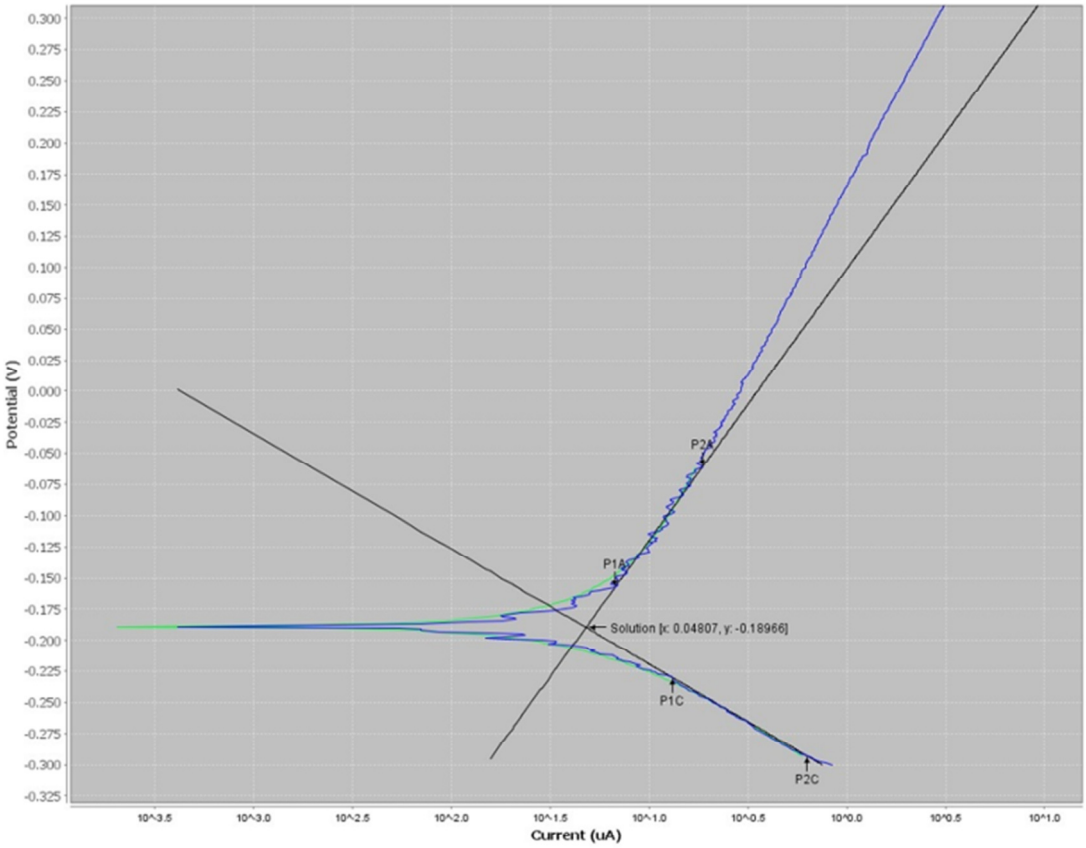

Corrosion Analysis

Selected points:

	Log(i)	V
1st anodic point:	0.07000	-0.15600
2nd anodic point:	0.16208	-0.07600
1st cathodic point:	0.13125	-0.23000
2nd cathodic point:	0.53292	-0.28800

Select new points

Results:

i corrosion	0.08870	µA
J corrosion	0.08870	µA/cm2
ba	0.12354	V/dec
bc	0.42790	V/dec
Rp	469.30138	KOhm
E corr, obs	-0.18900	V
E corr, calc	-0.18945	V
E begin	-0.28800	V
E end	-0.07600	V
Corrosion rate	0.00199	mm/year
	0.07851	mil/year

Copy to clipboard

Exit

Fig. 8. Tafel polarization curve and corrosion analysis results of Stellite 6 alloy laser cladding sample.

Following the stabilization phase, Linear Sweep Voltammetry (LSV) was performed over a potential range encompassing the E_{ocp} to determine the electrochemical characteristics of the coating. The LSV results were analyzed using the DropView 8400 software, incorporating the material-specific parameters of the Stellite 6 alloy: molar equivalent weight M = 59.5 (g/mol), density of alloy ρ= 8.44 (g/cm^3), and electrode surface area A = 1 cm^2. The polarization curve and associated corrosion parameters (corrosion potential E_{corr}, corrosion current I_{corr}, corrosion current density $J_{corr)}$ were extracted, as presented in Figure 8.

The electrochemical analysis revealed a corrosion potential E_{corr} of -0.189 V, indicating the thermodynamic tendency of the coating toward corrosion is low. The corrosion current density I_{corr} was exceptionally low, measured at 0.00887 µA/cm², corresponding to a calculated Corrosion Rate (CR) of 0.00199 mm/year. These results confirm that the Stellite 6 laser coating exhibits excellent corrosion resistance in a 3.5 wt.% NaCl environment.

To contextualize the performance, Table III compares the electrochemical corrosion parameters of the Stellite 6 coating with those of the uncoated AISI 1045 steel substrate, based on previous studies [13, 14].

TABLE III. ELECTROCHEMICAL PARAMETERS STELLITE 6 ALLOY COATING AND 1045 STEEL SUBSTRATE

Parameter	E_{corr} (V)	I_{Corr} (µA/cm^2)	CR (mm/year)	b_a (V/dec)	b_c (V/dec)
Substrate [14]	-0.660	35.8	0.421	0.1433	0.1047
Stellite 6	-0.189	0.0887	0.00199	0.1235	0.4279

The corrosion current density of 1045 steel is significantly higher than that of the Stellite 6 coating, demonstrating the coating's superior protective properties. Furthermore, the corrosion rate of 1045 steel is more than 200 times greater than that of the coated sample. The protection efficiency (PE%) of the Stellite 6 coating was calculated using the following equation [15]:

$$PE\% = \frac{I_{corr}(uncoated) - I_{corr}(coated)}{I_{corr}(uncoated)} \cdot 100\% \quad (1)$$

By substituting the corrosion current densities from Table III into the equation, the protection efficiency of the Stellite 6 coating was determined to be 99.75%.

IV. CONCLUSION

In this study, a Stellite 6 alloy coating was successfully deposited on 1045 medium-carbon steel using laser cladding. The microstructural evolution, mechanical properties, and electrochemical corrosion behavior of the coating were systematically investigated.

The microstructural analysis revealed a defect-free interface between the coating and the substrate, with no observable cracks or pores, indicating good metallurgical bonding. From the substrate–coating interface to the surface, the coating exhibited a gradient microstructure transitioning from planar to cellular and then to columnar dendritic and crystalline structures. The dendritic growth direction was aligned with the thermal gradient during solidification, extending from the interface toward the coating surface.

The coating demonstrated a relatively uniform microhardness, with an average value of 481.64 $HV_{0.3}$, which is approximately 2.8 times higher than the average hardness of the 1045 steel substrate. This significant increase in hardness indicates a substantial enhancement in the mechanical properties and wear resistance of the coated substrate.

Electrochemical corrosion testing in a 3.5 wt.% NaCl solution confirmed the excellent corrosion resistance of the Stellite 6 coating. The measured corrosion current density (I_{corr}) of the coating was only 0.00887 µA/cm^2, substantially lower than that of the uncoated 1045 steel. Additionally, the corrosion rate of the coating was approximately 200 times lower than that of the substrate. The calculated protection efficiency of the coating reached 99.75%, demonstrating the coating's outstanding capability to protect the substrate in a simulated seawater environment.

These results confirm that laser cladding with Stellite 6 is an effective method for significantly enhancing the surface performance of 1045 steel in terms of both mechanical and corrosion-resistant properties.

ACKNOWLEDGMENT

This research is funded by the University of Transport and Communications (UTC) under grant number T2025-CK-006.

REFERENCES

[1] T. Schopphoven, A. Gasser, K. Wissenbach, and R. Poprawe, "Investigations on ultra-high-speed laser material deposition as alternative for hard chrome plating and thermal spraying," *Journal of Laser Applications*, vol. 28, no. 2, May 2016, Art. no. 022501, https://doi.org/10.2351/1.4943910.

[2] M. S. Safavi and F. C. Walsh, "Electrodeposited Co-P alloy and composite coatings: A review of progress towards replacement of conventional hard chromium deposits," *Surface and Coatings Technology*, vol. 422, Sep. 2021, Art. no. 127564, https://doi.org/10.1016/j.surfcoat.2021.127564.

[3] J. N. Ndumia, M. Kang, B. V. Gbenontin, J. Lin, and S. M. Nyambura, "A Review on the Wear, Corrosion and High-Temperature Resistant Properties of Wire Arc-Sprayed Fe-Based Coatings," *Nanomaterials*, vol. 11, no. 10, Sep. 2021, Art. no. 2527, https://doi.org/10.3390/nano11102527.

[4] A. W. Fande, R. V. Taiwade, and L. Raut, "Development of activated tungsten inert gas welding and its current status: A review," *Materials and Manufacturing Processes*, vol. 37, no. 8, pp. 841–876, Jun. 2022, https://doi.org/10.1080/10426914.2022.2039695.

[5] L. Zhou *et al.*, "Research status and prospect of extreme high-speed laser cladding technology," *Optics & Laser Technology*, vol. 168, Jan. 2024, Art. no. 109800, https://doi.org/10.1016/j.optlastec.2023.109800.

[6] L. C. Dang, C. V. Nguyen, A. H. Le, and D. T. Bui, "A Study on the Influence of Printing Orientation in Metal Printing Using Material Extrusion Technology on the Mechanical Properties of 17-4 Stainless Steel Products," *Journal of Machine Engineering*, vol. 23, no. 4, pp. 89–100, Dec. 2023, https://doi.org/10.36897/jme/170509.

[7] Y. Liu, Y. Ding, L. Yang, R. Sun, T. Zhang, and X. Yang, "Research and progress of laser cladding on engineering alloys: A review," *Journal of Manufacturing Processes*, vol. 66, pp. 341–363, Jun. 2021, https://doi.org/10.1016/j.jmapro.2021.03.061.

[8] K. Wang, Z. Zhang, D. Xiang, and J. Ju, "Research and Progress of Laser Cladding: Process, Materials and Applications," *Coatings*, vol. 12,

no. 10, Sep. 2022, Art. no. 1382, https://doi.org/10.3390/coatings 12101382.

[9] M. Kiehl, A. Scheid, K. Graf, B. Ernst, and U. Tetzlaff, "Coaxial Laser Cladding of Cobalt-Base Alloy Stellite™ 6 on Grey Cast Iron Analysis of the Microstructural and Mechanical Properties Depending on the Laser Power," *Journal of Materials Engineering and Performance*, vol. 32, no. 8, pp. 3821–3838, Apr. 2023, https://doi.org/10.1007/s11665-022-07358-3.

[10] F. X. Huang, Z. H. Jiang, X. M. Liu, J. S. Lian, and L. Chen, "Effects of Process Parameters on Microstructure and Hardness of Layers by Laser Cladding," *ISIJ International*, vol. 51, no. 3, pp. 441–447, 2011, https://doi.org/10.2355/isijinternational.51.441.

[11] E. R. I. Mahmoud and H. F. El-Labban, "Microstructure and Wear Behavior of TiC Coating Deposited on Spheroidized Graphite Cast Iron Using Laser Surfacing," *Engineering, Technology & Applied Science Research*, vol. 4, no. 5, pp. 696–701, Oct. 2014, https://doi.org/10.48084/etasr.483.

[12] V. P. Vijeesh, M. R. Ramesh, and A. D. Anoop, "Inconel 625 Coatings on AISI 304 Steel using Laser Cladding: Microstructure and Hardness," *Engineering, Technology & Applied Science Research*, vol. 13, no. 5, pp. 11911–11916, Oct. 2023, https://doi.org/10.48084/etasr.6297.

[13] H. Liu, C. Wang, X. Zhang, Y. Jiang, C. Cai, and S. Tang, "Improving the corrosion resistance and mechanical property of 45 steel surface by laser cladding with Ni60CuMoW alloy powder," *Surface and Coatings Technology*, vol. 228, pp. S296–S300, Aug. 2013, https://doi.org/10.1016/j.surfcoat.2012.05.115.

[14] W. Wu, R. Chen, Z. Yang, Z. He, Y. Zhou, and F. Lv, "Corrosion resistance of 45 carbon steel enhanced by laser graphene-based coating," *Diamond and Related Materials*, vol. 116, Jun. 2021, Art. no. 108370, https://doi.org/10.1016/j.diamond.2021.108370.

[15] E. Ghiamati Yazdi, Z. S. Ghahfarokhi, and M. Bagherzadeh, "Protection of carbon steel corrosion in 3.5% NaCl medium by aryldiazonium grafted graphene coatings," *New Journal of Chemistry.*, vol. 41, no. 21, pp. 12470–12480, 2017, https://doi.org/10.1039/C7NJ01655G.